Biochimica et Biophysica Acta (BBA) - Bioenergetics, 1837 (6): 849–856, 2014
DOI: 10.1016/j.bbabio.2014.01.005 (§)

Effect of TMAO and Betaine on the Energy Landscape of Photosystem I

Jana B. Nieder[†‡], Martin Hussels[⋆*], Robert Bittl[†], Marc Brecht[⋆○#]

[†] *Fachbereich Physik, Freie Universität Berlin, Arnimallee 14,14195 Berlin, Germany*

[‡] *present address: ICFO - Institut de Ciencies Fotoniques, Av. Carl Friedrich Gauss 3, 08860 Castelldefels, Barcelona, Spain*

[⋆] *Universität Tübingen, IPTC and Lisa+ Center, Auf der Morgenstelle 18, 72076 Tübingen, Germany*

[*] *present address: Physikalisch-Technische Bundesanstalt, Abbe Str. 2-12, 10587 Berlin, Germany*

[○] *Zurich University of Applied Sciences, Technikumstrasse 13, 8401 Winterthur, Switzerland*

[#] To whom correspondence should be addressed. E-mail, marc.brecht@uni-tuebingen.de; phone,+49-7071-29-76239; fax +49-7071-29-5490.

Abstract

The accumulation of organic co-solvents in cells is a basic strategy for organisms from various species to increase stress tolerance in extreme environments. Widespread representatives of this class of co-solvents are trimethylamine-N-oxide (TMAO) and betaine; these small molecules are able to stabilize the native conformation of proteins and prevent their aggregation. Despite their importance, detailed experimental studies on the impact of these co-solvents on the energy landscape of proteins have not yet been carried out. We use single-molecule spectroscopy at cryogenic temperatures to examine the influence of these physiological relevant co-solvents on photosystem I (PSI) from *Thermosynechococcus elongatus*. In contrast to PSI ensemble spectra, which are almost unaffected by the addition of TMAO and betaine, statistical analysis of the fluorescence emission from individual PSI trimers yields insight into the interaction of the co-solvents with PSI. The results show an increased homogeneity upon addition of TMAO or betaine. The number of detectable zero-phonon lines (ZPLs) is reduced, indicating spectral diffusion processes with faster rates. In the framework of energy landscape model these findings indicate, co-solvents lead to reduced barrier heights between energy valleys, and thus efficient screening of protein conformations can take place.

TOC Graphic

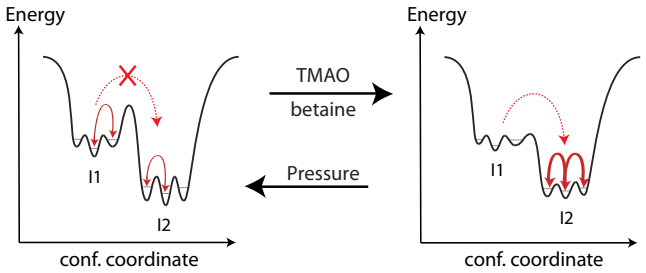
Energy
I1
I2
conf. coordinate
TMAO
betaine
Pressure
Energy
I1
I2
conf. coordinate

Introduction

The proper function of proteins is a prerequisite for life. Thermodynamic parameters such as temperature, pressure and pH value are important for description of macroscopic protein properties, but they fail to assist in understanding proteins at the molecular level. One of the most important factors are the structure and dynamics of water close to the surface of proteins (hydration layer) [1, 2]. The hydration layer's properties depend not only on the electrostatics of the protein surface itself, but also on various co-soluted small molecules present in living organisms. Such additives can be small water-miscible organic molecules (co-solvents). These additives show remarkable effects on structure and function of proteins [3, 4]. Organisms and tissues accumulate co-solvents intracellularly to offset the effect of water stress, e.g., an abnormal increase in osmolality (hyperosmolality) and hydrostatic pressure [3, 5]. Co-solvents widen the range wherein organisms can adapt protein function and they enable nature to use proteins with virtually unaltered amino-acid sequence in drastically different environmental conditions. Specifically, the accumulation of co-solvents, such as TMAO and betaine, is observed when cells or tissues are subjected to osmotic or water stress resulting from exposure to high salinity, high hydrostatic pressures and desiccation or dehydration [4, 6]. It seems that evolution chose a genetic simplistic strategy to cope against such stress conditions [7]. Therefore, the influence of these molecules motivated experimental and theoretical groups to take a closer look at the molecular details of their interaction with proteins [8–17].

The general concept to control the functional protein structure via co-solvents has been transferred to *in vitro* studies [3]. While protective co-solvents like TMAO and betaine push the equilibrium of protein folding towards the native form [18, 19], denaturing co-

solvents like urea push it towards the unfolded form [20, 21]. Due to their protective properties, TMAO and especially betaine are often used as stabilizing agents during protein crystallization and purification [22, 23].

It has been found that the stress tolerance of organisms, which intrinsically do not make use of co-solvents, can be increased by transgenetic implementation of co-solvents. To this end various biosynthetic pathways e.g. for betaine have been identified [18] and implemented into various model organisms. Such transgenetic modified plants show faster physiological development and a gain in stress tolerance, including salt stress, low and high temperature stress and high intensity light stress (for a Review see [19] and references therein).

In this study we investigate the influence of two very abundant co-solvents, TMAO and betaine (for the chemical structures see Figure 1), on the conformational dynamics of the large membrane protein complex, photosystem I (PSI). Both co-solvents are widely spread in biological organisms. TMAO is e. g. found in marine animals, where the content of TMAO in their muscle cells is correlated with the sea level where the various organisms are typically found. Deep-sea fish has higher concentration of TMAO than shallow water populations, and therefore TMAO was supposed to act besides others as a protectant against high-pressure denaturation [24]. Betaine is present in various organisms including animals and plants and is widely spread for *in vitro* protein stabilization [19].

PSI – a key part of the photosynthetic apparatus – is taken here as a model protein complex (trimeric protein structure is shown in Figure 2A). Its high and reliable sample quality and preferential optical properties [26] are of advantage and are briefly outlined in the following. The PSI antenna system consists of ∼90 chlorophyll *a* molecules that form a very efficient

exciton transfer network [27, 28]. The arrangement of the chlorophyll *a* molecules allows for PSI excitation at the absorption maximum (∼680 nm), far from the absorption of "P700" pigments at 700 nm which are responsible for primary PSI photochemistry (see also Figure 2B) [29, 30]. A portion of the chlorophyll *a* molecules show lower site energies than P700 [33]. These low-energy pigments are often called the "red pools" or the "red-most" chlorophylls (for a review, see Gobets et al. [30] and Karapetyan et al. [29]). At low temperatures, several of these chlorophylls can be observed by their fluorescence emission (Figure 2B) [33–36]. The fluorescence maximum is found at around 730 nm resulting in a red shift of almost 50 nm between the main absorption of PSI (Q_y-band) as shown in Figure 2C. This large red shift is advantageous for any kind of fluorescence-based studies because the entire emission can be observed without restrictions with the suited filter sets.

Protein-embedded chromophores like chlorophylls in light-harvesting systems can be used as native sensors inside proteins. In several cases, the fluorescence emission of such chromophores can be detected down to the single-molecule level [37–39]. At room temperature, spectral diffusion and photo bleaching hamper the collection of detailed conformational information [40–43]. Lowering the temperature reduces the impact of spectral diffusion [43–45] and the emission profile of a single emitter composed of a sharp zero-phonon line (ZPL) and a phonon wing becomes observable [46–49].

The conformational dynamics of proteins occur on a complex, rugged energy landscape characterized by a large number of different conformational substates, as shown by the pioneering experiments on myoblobin by Frauenfelder et al. [50]. For protein-embedded chromophores, this environment cannot be simply reduced to the pocket wherein the chromophore is bound; the properties of the whole protein have to be taken into account. The

conformational substates correspond to local minima in the potential energy surface. Transitions between different nearly isoenergetic states in such a rugged energy landscape of a protein have a direct influence on the absorption and emission properties of chromophores embedded into the protein environment. Therefore protein-embedded chromophores can be used as sensitive probes of the changes in the conformation of proteins.

In prior studies we used the optical properties of the protein-embedded chromophores on the one hand side for the investigation of the local dynamics inside the protein binding pockets, as well as, for the analysis of overall protein conformations. By H_2O to D_2O exchange a remarkable influence of H-bridges between the protein scaffold and the bound chromophores on the rate of spectral diffusion was observed [51]. The effects on the overall conformation of PSI were studied under the influence of glycerol and Polyphenyl-alcohol (PVA), which are typical additives for low temperature spectroscopy and single-molecule studies of proteins, respectively. High concentration of glycerol leads to remarkable homogenization of the proteins, whereas embedding of PSI into a PVA matrix yields an increased heterogeneity of the proteins accompanied by a partial denaturation [52, 53].

In this work we investigate the influence of physiological relevant co-solvents (TMAO and betaine) by a combination of single-molecule spectroscopy and statistical analysis. This approach opens the possibility to correlate fluorescence emission changes with conformational properties of the proteins inducing by the addition of the co-solvent to the respective buffer solutions.

1 Material and Methods

PSI trimers from *T. elongatus* were isolated as described in Ref [54]. Then the purified PSI trimers were diluted in buffer solution (pH 7.5) containing 20 mM Tricine, 25 mM $MgCl_2$, and 0.4 mM β-DM as detergent, to reach a chlorophyll *a* concentration of $\sim$20 μM. This amount of detergent is adequate for the critical solubilization concentration for a PSI trimer concentration of 0.5 μM to avoid PSI aggregation [55].

PSI samples in buffer solution as used for the single-molecule experiments were further diluted in a Tricine-buffer solution containing 20 mM Tricine, 25 mM $MgCl_2$, 0.4 mM β-DM, and 5 mM sodium ascorbate in milli-Q water. Sodium ascorbate was added for pre-reduction of P700. In case of the Trimethylamine-N-oxide(TMAO)- and betaine-containing samples, the buffer solution used for diluting the PSI sample additionally contained 1M TMAO or 1M betaine respectively. The final PSI trimer concentration was $\sim$3 pM. Less than 1 μL of these samples were placed between coverslips for single-molecule experiments. Sample preparation and mounting were accomplished under indirect light. Finally, the samples were transferred directly into the cryostat and rapidly plunged into liquid helium. Experiments were carried out using a home-built confocal microscope operating at 1.4 K. For imaging of single molecules, a piezo tip tilt module (Physik Instrumente PI S-334.2SL) was used to deflect beams. The excitation source was a diode laser (680nm Schäfter & Kirchhoff). The fluorescence emission was detected using either an avalanche photodiode (Perkin-Elmer SPCM-AQR-15, <50 dark counts/s) for fast integral fluorescence detection, or an Acton Research 30 cm spectrograph (Acton SpectraPro308) equipped with a back-illuminated CCD camera (Roper Scientific Spec-10:100BR/LN) for recording fluorescence spectra. Stray laser light was blocked by a Raman long-pass filter (AHF HQ695LP). For

illumination and detection, the same microscope objective (60×, N.A. 0.8 JIS, Edmund Optics) was employed and immersed in liquid helium. A laser intensity of 100 μW, measured behind the scanning module, was used for excitation. In a sequence of spectra, the usual exposure time for each spectrum was 1 s, resulting in a typical S/N ratio of > 6 for single PSI complexes at the given excitation power, referred to as time resolution in the following context.

The algorithm used for the determination of the ZPLs in time dependent spectral series is described in detail in [52]. In short, it includes a smoothing of the spectra series in two dimensions (wavelength and time) using a moving average filter as provided in Matlab (Curve Fitting Toolbox), a standard Laplace 1D edge filter is applied in the wavelength domain to enhance sharp and to suppress broad structures. For all spectra series wavelength positions are collected where the intensity surpasses a certain threshold, which implies the presence of a narrow line feature in the spectra.

2 Results

PSI complexes were analyzed as prepared in buffer solution, buffer solution with TMAO and buffer solution with betaine. In total we recorded spectral information for 137 PSI complexes (trimers) in buffer solution, 110 in TMAO-containing and 122 in betaine-containing buffer solution. The average spectra taken over all investigated PSI trimers per sample preparation are shown in Figure 3. The fluorescence intensity maxima for the different preparations are found at: 726.5±0.5 nm (buffer solution), 727±0.5 nm (TMAO), and 727.5±1.0 nm (betaine) see also Table 1 where these values are listed together with values

for PSI preparations containing PVA and glycerol. The variations in the average emission spectra between the preparations are very subtle compared to other sample preparations of PSI, as for example in glycerol or PVA containing buffer solutions (see Figure 4 and Ref.[52]).

In contrast, on the single-complex level a high variance of spectral fingerprints characteristic for each individual PSI complex is found. These variations concern shape and wavelength position of the broad intensity distribution, and wavelength position, number and intensity of the visible ZPLs. In Figure 4 three spectra are given for each sample preparation and for comparison representative single-complex spectra for PSI in glycerol (taken from Ref: [53]) are shown. The heterogeneity between the spectra from individual complexes, is comparably high in buffer solution as well as in TMAO and in betaine solution compared to observations made e.g. in glycerol-containing sample preparations (Figure 4 and Ref. [53]).

For PSI in H_2O-based buffer solution variations are found for the maximum position of the broad fluorescence emission contributions, in the three examples peaking at 733 nm, 732 nm and 722 nm (Figure 4, red curves). Narrow line contributions are additionally found with strong heterogeneity concerning the relative intensity compared to the broad contributions. The ZPL in the upper spectrum at 710 nm exceeds the peak maximum at 732 nm of the broad contribution, and for the lower spectrum a narrow line with a relatively high intensity is found at a long wavelength position at 732 nm sticking out of the underlying broad contribution. Other narrow line features stay far below in intensity, e.g. the contributions found at around 708 nm in the middle spectrum and at 705 nm and 734 and 740 nm in the lower spectrum.

The representative example spectra for single PSI-complexes measured in TMAO-containing buffer are similarly characterized by heterogeneity (Figure 4, shown in green), while the number of detected narrow line features is smaller. The narrow line features detected at 710 nm and 712 nm in the upper spectrum are positioned on top of a broader band, and the relative intensity of the narrow features in the middle and lower spectra are very low compared to the intensity in the broader contributions. Maxima of the broad contributions are heterogenous and positioned at around 740 nm, 728 nm 736 nm for the spectra from top towards the bottom.

Example spectra for single PSI complexes in betaine show less narrow line contributions. In the middle spectrum a well resolved narrow line is found at 711 nm and a slightly broader contribution with low relative intensity at 713 nm in the bottom spectrum (Figure 4, shown in dark blue). The upper spectrum shows two broad distributions with maxima at 720 nm and 728 nm. Again the maxima positions of the broad components vary from spectrum to spectrum for the different individual complexes. Maxima are found at 730 nm and 732 nm for the middle and lower spectrum, respectively.

The influence of glycerol on PSI was described recently in Ref. [53]. Example spectra have been taken from Ref. [53] to highlight the difference of the effect of glycerol on the spectral properties of PSI compared to the effects of TMAO and betaine (Figure 4, shown in cyan). The spectral shift to longer wavelength in the average spectrum over many molecules (see Figure 3) is reflected by the strong homogeneity of the peak position of the broad spectral contribution even on the single complex level. In all three spectra shown, the maxima are at $\sim$730 nm. Only on the short wavelength side of the broad contribution spectral variances are present due to various ZPLs with rather low relative intensity.

To detect overall differences in the various spectra of individual PSI complexes dependent on the presence of the co-solvents in the buffer, we chose a statistical approach with an algorithm-based analysis, which has been described in detail in Ref. [52]. One algorithm is used to determine the wavelength position of the most intense contribution in the fluorescence spectra of each individual PSI complex together with its full width at half maximum (FWHM). These parameters are determined regardless whether the intense contribution is a ZPL or a broad distribution. The result of this analysis applied on the fluorescence emission spectra for all single PSI trimers of the three sample types are summarized in 2D-histogram-scatter plots in Figure 5. The histograms on the upper panels are the projections of the identified contributions found on given wavelength intervals, while the histograms on the right of the scatter plot are the projections along the axis representing the associated FWHM values of the respective high intensity contributions. The histograms are used to map the statistical distributions, which are not accessible when scatter points are overlapping.

For all PSI samples the highest intensity in a single complex spectrum is found within a large wavelength interval extending from 705 – 740 nm for PSI in buffer and 705 – 742 nm in case of TMAO and 705 – 739 nm in case of betaine. The biggest difference when comparing the histograms along the wavelength axis for the different preparations, is found in the shape of the distributions. For PSI in buffer two maxima are found at around 710 nm and 727 nm, while in the case of TMAO and betaine the subpopulation around 727 nm becomes dominant and is reflected in a very sharp peak indicating increased relative occurrence of this contribution while no shorter wavelength contribution is giving rise to a second peak but an unstructured plateau covers the lower wavelength range.

Significant differences are found in the histograms along the FWHM axis of the scatter plots. For PSI in buffer two independent contributions are found, one with small width of <10 nm FWHM and another peaking at around 20 nm FWHM. While the broad contribution is similarly found for PSI in TMAO and betaine, the narrow line contributions are virtually absent (only two events were detected for the TMAO-containing sample and none in case of betaine). In the scatter plots the various identified intense spectral components are spread point by point along the wavelength position and FWHM coordinates. In case of PSI in buffer three point clouds are formed. One rather confined point cloud with a center at (710 nm/2 nm) (wavelength position/FWHM), another broad point cloud around (727 nm/25 nm) and a third point cloud representing high intensity contributions positioned at relatively long wavelength positions and with narrow line widths found at around (734 nm/<10 nm). This third spectral contribution is completely absent in the PSI preparations with the co-solutes TMAO and betaine, respectively.

For all individual PSI complexes also time-dependent spectra sequences were recorded with 1 s acquisition time per spectrum. In Figure 6 a typical time-dependent spectral data set taken for an individual PSI complex is shown together with the associated average spectrum and the extracted ZPL information (here PSI in TMAO). The time-dependent spectra are characterized by complex dynamic behavior (see Figure 6B). The fluorescence emission of PSI is composed of the different contributions associated to the different red chlorophyll states [39]. The narrow line contributions either shiver (e.g. at around 699 nm and 709 nm for the PSI complex shown in Figure 6) or jump along the wavelength axes over time (e.g. after 22 s and 83 s of observation time). For the broad contributions, solvent isotope exchange experiments revealed that these can arise because of very fast spectral diffusion

dynamics happening on a much faster time scale than seconds [51], and thus underlying dynamics cannot be directly resolved in our measurements with 1 s time resolution. The theoretical line shapes expected for the different single emitters in PSI [56, 57], without broadening by spectral diffusion, are added to the average spectrum taken over the spectral series in Figure 6A.

A way to obtain kinetic information from the recorded time-dependent spectral series is to analyze the number of ZPL features being resolved in these series. By analyzing the occurrence of ZPLs we directly map the probability for slow spectral diffusion with respect to the time resolution of 1 s. A ZPL feature is only identified, when the spectral contribution shows stability in a time interval >1 s. To identify ZPL contributions we use an algorithm-based analysis (see MM and Ref. [52]). The ZPL positions extracted for all investigated individual PSI complexes are visualized as histograms (see Figure 7). All ZPL distributions show the highest amount of ZPLs in the spectral region < 720 nm. The center positions and widths of the distributions were determined by fitting with one Gaussian. The centers are found at 710.4 nm (buffer), 710.2 (TMAO), and 711.6 (betaine); the widths are 4.1 nm for buffer solution and TMAO, and 6.2 nm for betaine. At wavelength > 720 nm, ZPLs are observed for around 30% of the complexes in buffer solution, whereas the observation of ZPLs remains an exception for TMAO and betaine. On average, 1.6 (buffer), 0.7 (TMAO), and 0.9 (betaine) ZPLs per data set were observed. The extracted information is summarized inTable 2 together with analog information determined on PVA and glycerol-containing PSI samples. While the center position of the distributions is for all sample preparations around 710 nm, for the co-solute containing samples with TMAO and betaine in the buffer composition a strongly reduced detection of ZPL contributions is apparent. PVA samples

are the only PSI preparations which lead to increased ZPL detection in the spectra of single PSI complexes compared to simple buffer preparations [52].

3 Discussion

The shape of the emission spectrum of PSI can be changed remarkably by the solution wherein PSI is solubilized. The addition of glycerol causes a shift of the maximum by several nanometers and a change of the emission shape in the region 710 – 720 nm (Figure 3, cyan curve) [52]. If TMAO or betaine is added, the observed effects are much smaller (blue, green and red curves). Spectral changes induced by TMAO/betaine can be resolved by single-molecule spectroscopy at low temperatures (Figure 4). The observed spectral fluctuations of the fluorescence emission of single PSI trimers are caused by conformational changes of the protein during the experiments which corresponds to a motion between different valleys in the energy landscape [38, 39]. A ZPL detection event can be associated with a rather trapped protein conformation, where lacking conformational changes lead to spectral stability of the protein embedded emitter. The observed width of the ZPL distribution can be used as a measure for protein heterogeneity in the sample [52, 53]. Two statistical methods were used to evaluate the heterogeneity of PSI emission spectra. These methods allow on the one hand the determination of the most intense contributions in the spectra (Figures 5) and on the other hand the identification of ZPL contributions (Figure 6, 7). Strongly reduced intense ZPL contributions as well as reduced abundance of ZPLs are observed for TMAO and betaine preparations compared to PSI in buffer solution. The overall statistics of ZPLs determined from time-resolved data additionally shows a reduced

number of ZPLs per PSI complex at longer wavelength positions (Table 2 and Figure 7).

Most of the red-pool chlorophylls are buried within the proteins scaffolds [32]. For these chromophores, a large change of their lifetime induced by TMAO or betaine in the solution can be ruled out. Changed spectral overlap between the energetically higher lying chlorophyll states (referred to as C708 states) and the lower lying states are a reasonable source for the reduced emission of C708 as observed by a smaller number of high intensity contributions around 710 nm and in average a smaller number of ZPL detection at this wavelength position. The slight differences between the average spectra for TMAO/betaine and buffer solution between 710 – 725 nm and the red part of the spectrum $>$ 735 nm (Figure 3) are an indication for such types of changes.

Heterogeneity of the emission profiles in the region of the intense ZPLs is comparably high for PSI in buffer solution. States with slow energy transfer and intense ZPLs as well as conformational states with fast energy transfer and no ZPLs are present. In the case of PSI in TMAO and betaine these variations are much lower and the wavelength range in which ZPLs are found is much smaller. Thus, it seems that the ZPLs of C708 are squeezed into a smaller wavelength range (Figure 5, 7). A reduced heterogeneity of the conformational states is a plausible explanation for the observed effects [58].

The number of ZPLs for wavelengths >720 nm (Figure 7) also varies between preparations. In buffer solution, a certain fraction of data sets show ZPLs. The probability of observing ZPLs in this spectral region is much lower due to fast spectral diffusion and strong electron-phonon coupling of the involved chromophores [39, 51]. These chromophores change their site energies several times during the accumulation time. An electron-phonon coupling of $S \sim 2.2$ was predicted for these states [36], yielding a ZPL/phonon wing intensity ratio

of ∼0.14. The increase of intensity in the broad phonon wings at the expense of ZPLs further complicates their detection. The already low probability of observing ZPLs drops completely if TMAO/betaine is added to the solution, indicating a further increase of the spectral diffusion rates.

As illustrated Figure 8 an increase of spectral diffusion indicates a decreased barrier height between the different conformational states in the energy valleys, or – in other words – increased protein flexibility [59, 60]. In the presence of co-solutes conformational states can be accessed more easily, which renders the protein more flexible. On the other side, the probability that a protein gets stuck in one conformational state surrounded by high energy barriers becomes less likely. Application of hydrostatic pressure on proteins can change the curvature of the energy landscape [61] and alter the height of the barriers between the substates. These changes can be interpreted as an increased roughness of the energy landscape (Figure 8). Several sub-conformations can be trapped by applying pressure; the barriers separating these states become too high to be crossed. The increase of roughness by pressure is used, for instance, to study intermediates in protein folding [62]. Trapping of a certain fraction of the proteins in different states yields an increased heterogeneity of the whole ensemble. TMAO and betaine are found in high concentration in animals living under high hydrostatic pressure [5, 63]. Based on the presented data, it can be assumed that organisms use TMAO/betaine as protective agents to counteract the negative effect of pressure. TMAO/betaine co-solvents may protect the native shape of the energy landscape and make protein function possible under inhospitable conditions.

In conclusion, the average fluorescence emission of sets of single PSI trimers prepared in

buffer and buffer with 1M TMAO and 1M betaine are almost identical. Statistical analysis of spectra from single PSI trimers uncovered the effects of TMAO and betaine on protein energy landscapes. With the addition of TMAO and betaine the spectral window for ZPL detection is reduced. A fraction of conformational states wherein the protein can be trapped under native conditions seems to be effectively suppressed. Increased spectral diffusion rates lower the likelihood of observing ZPLs, indicating a more flexible protein structure. Within the framework of protein energy landscapes both effects can be explained by a reduced roughness of the energy valleys. This effect yields a suppression of intermediate states and increased spectral diffusion (see Figure 8). Interestingly, high concentrations of TMAO and betaine are found in animals living under high hydrostatic pressure, which is known to increase the heterogeneity and energy landscape roughness. TMAO and betaine counteract the effects of pressure and can restore native protein function. This may be one reason why animals utilize a high amount of these co-solvents under inhospitable living conditions.

4 Acknowledgement

We thank Eberhard Schlodder for the PSI samples and helpful discussions. This work was supported by the Heisenberg-Programm of the Deutsche Forschungsgemeinschaft DFG (BR 4102/1-1 and BR 4102/2-1).

References

1. M. Tarek, D. J. Tobias, Environmental dependence of the dynamics of protein hydration water, Journal of the American Chemical Society 121 (41) (1999) 9740–9741.

2. H. Nakagawa, M. Kataoka, Percolation of hydration water as a control of protein dynamics, Journal of the Physical Society of Japan 79 (8) (2010) 083801.

3. P. H. Yancey, Organic osmolytes as compatible, metabolic and counteracting cytoprotectants in high osmolarity and other stresses, Journal of Experimental Biology 208 (15) (2005) 2819–2830.

4. M. B. Burg, J. D. Ferraris, Intracellular organic osmolytes: Function and regulation, Journal of Biological Chemistry 283 (12) (2008) 7309–7313.

5. P. H. Yancey, M. D. Rhea, K. M. Kemp, D. M. Bailey, Trimethylamine oxide, betaine and other osmolytes in deep-sea animals: Depth trends and effects on enzymes under hydrostatic pressure, Cellular And Molecular Biology 50 (4) (2004) 371–376.

6. T. Y. Lin, H. Z., S. N. Timasheff, Why do some organisms use a urea-methylamine mixture as osmolyte - thermodynamic compensation of urea and trimethylamine n-oxide interactions with protein, Biochemistry 33 (42) (1994) 12695–12701.

7. P. H. Yancey, M. E. Clark, S. C. Hand, R. D. Bowklus, G. N. Somero, Living with water stress evolution of osmolyte systems, Science (Washington D C) 217 (4566) (1982) 1214–1222.

8. J. F. Back, D. Oakenfull, M. B. Smith, Increased thermal-stability of proteins in the presence of sugars and polyols, Biochemistry 18 (23) (1979) 5191–5196.

9. A. Ansari, C. M. Jones, E. R. Henry, J. Hofrichter, W. A. Eaton, The role of solvent viscosity in the dynamics of protein conformational-changes, Science 256 (5065) (1992) 1796–1798.

10. G. S. Lakshmikanth, G. Krishnamoorthy, Solvent-exposed tryptophans probe the dynamics at protein surfaces, Biophysical Journal 77 (2) (1999) 1100–1106.

11. S. N. Timasheff, Protein-solvent preferential interactions, protein hydration, and the modulation of biochemical reactions by solvent components, Proceedings of the National Academy of Sciences of the United States of America 99 (15) (2002) 9721–9726.

12. Q. Zou, B. J. Bennion, V. Daggett, K. P. Murphy, The molecular mechanism of stabilization of proteins by tmao and its ability to counteract the effects of urea., Journal of the American Chemical Society 124 (7) (2002) 1192–1202.

13. R. C. Zinober, D. J. Brockwell, G. S. Beddard, A. W. Blake, P. D. Olmsted, S. E. Radford, D. A. Smith, Mechanically unfolding proteins: The effect of unfolding history and the supramolecular scaffold, Protein Science 11 (12) (2002) 2759–2765.

14. P. W. Fenimore, H. Frauenfelder, B. H. McMahon, R. D. Young, Bulk-solvent and hydration-shell fluctuations, similar to alpha- and beta-fluctuations in glasses, control protein motions and functions, Proceedings of The National Academy of Sciences of The United States of Americaf The National Academy of Sciences of The United States of America 101 (40) (2004) 14408–14413.

15. F. F. Liu, L. Ji, L. Zhang, X. Y. Dong, Y. Sun, Molecular basis for polyol-induced protein stability revealed by molecular dynamics simulations, Journal of Chemical Physics 132 (22) (2010) 225103–1 – 225103–9.

16. V. Vagenende, M. G. S. Yap, B. L. Trout, Mechanisms of protein stabilization and prevention of protein aggregation by glycerol, Biochemistry 48 (46) (2009) 11084–11096.

17. C. Malardier-Jugroot, D. T. Bowron, A. K. Soper, M. E. Johnson, T. Head-Gordon, Structure and water dynamics of aqueous peptide solutions in the presence of co-solvents, Physical Chemistry Chemical Physics 12 (2) (2010) 382–392.

18. S. J. Coughlan, R. G. W. Jones, Glycinebetaine biosynthesis and its control in detached secondary leaves of spinach, Planta 154 (1) (1982) 6–17.

19. A. Sakamoto, N. Murata, Genetic engineering of glycinebetaine synthesis in plants: current status and implications for enhancement of stress tolerance, Journal of Experimental Botany 51 (342) (2000) 81–88.

20. T. O. Street, D. W. Bolen, G. D. Rose, A molecular mechanism for osmolyte-induced protein stability, Proceedings of the National Academy of Sciences of the United States of America 103 (38) (2006) 13997–14002.

21. C. C. Lenky, C. J. McEntyre, M. Lever, Measurement of marine osmolytes in mammalian serum by liquid chromatography-tandem mass spectrometry, Analytical Biochemistry 420 (1) (2012) 7–12.

22. G. C. Papageorgiou, N. Murata, The unusually strong stabilizing effects of glycine betaine on the structure and function of the oxygen-evolving photosystem-II complex, Photosynthesis Research 44 (3) (1995) 243–252.

23. H. Marshall, M. Venkat, N. S. H. L. Seng, J. Cahn, D. H. Juers, The use of trimethylamine n-oxide as a primary precipitating agent and related methylamine osmolytes

as cryoprotective agents for macromolecular crystallography, Acta Crystallographica Section D-biological Crystallography 68 (2012) 69–81.

24. M. Gillett, J. Suko, F. Santoso, P. Yancey, Elevated levels of trimethylamine oxide in muscles of deep-sea gadiform teleosts: A high-pressure adaptation?, Journal of Experimental Exp. Zoo. 279 (4) (1997) 386–391.

25. R. M. C. Dawson, D. C. Elliott, W. H. Elliott, K. M. Jones, Data for Biochemical Research, Oxford University Press, 1959.

26. M. Brecht, Spectroscopic characterization of photosystem I at the single-molecule level, Molecular Physics 107 (2009) 1955–1974.

27. G. D. Scholes, X. J. Jordanides, G. R. Fleming, Adapting the Förster theory of energy transfer for modeling dynamics in aggregated molecular assemblies, Journal of Physical Chemistry B 105 (8) (2001) 1640–1651.

28. M. Byrdin, P. Jordan, N. Krauss, P. Fromme, D. Stehlik, E. Schlodder, Light harvesting in photosystem I: Modeling based on the 2.5-Angstrom structure of photosystem I from Synechococcus elongatus, Biophysical Journal 83 (1) (2002) 433–457.

29. N. V. Karapetyan, E. Schlodder, R. van Grondelle, J. P. Dekker, Advances in Photosynthesis and Respiration vol. 24, Photosystem I: The Light-Driven Plastocyanin:Ferredoxin Oxidoreductase, Springer, 2006.

30. B. Gobets, R. van Grondelle, Energy transfer and trapping in photosystem I, Biochimica et Biophysica Acta 1507 (1-3) (2001) 80–99.

31. P. Fromme, P. Jordan, N. Krauss, Structure of photosystem I, Biochim. Biophys. Acta, Bioenerg. 1507 (1-3) (2001) 5–31.

32. E. Schlodder, M. Hussels, M. Cetin, N. V. Karapetyan, M. Brecht, Fluorescence of the various red antenna states in photosystem I complexes from cyanobacteria is affected differently by the redox state of P700., Biochimica et Biophysica Acta 1807 (11) (2011) 1423–31.

33. E. Schlodder, V. V. Shubin, E. El-Mohsnwy, M. Rogner, N. V. Karapetyan, Steady-state and transient polarized absorption spectroscopy of photosystem I complexes from the cyanobacteria *Arthrospira platensis* and *Thermosynechococcus elongatus.*, Biochim. Biophys. Acta, Bioenerg. 1767(6) (2007) 732–741.

34. L. O. Palsson, J. P. Dekker, E. Schlodder, R. Monshouwer, R. van Grondelle, Polarized site-selective fluorescence spectroscopy of the long-wavelength emitting chlorophylls in isolated photosystem I particles of Synechococcus elongatus, Photosynthesis Research 48 (1-2) (1996) 239–246.

35. M. Byrdin, I. Rimke, E. Schlodder, D. Stehlik, T. A. Roelofs, Decay kinetics and quantum yields of fluorescence in photosystem I from synechococcus elongatus with P700 in the reduced and oxidized state: Are the kinetics of excited state decay trap-limited or transfer-limited?, Biophysical Journal 79 (2) (2000) 992–1007.

36. V. Zazubovich, S. Matsuzaki, T. W. Johnson, J. M. Hayes, P. R. Chitnis, G. J. Small, Red antenna states of photosystem I from cyanobacterium Synechococcus elongatus: a spectral hole burning study, Chemical Physics 275 (1-3) (2002) 47–59.

37. F. Jelezko, C. Tietz, U. Gerken, J. Wrachtrup, R. Bittl, Single-molecule spectroscopy on photosystem I pigment-protein complexes, J. Phys. Chem. B 104 (34) (2000) 8093–8096.

38. C. Hofmann, T. J. Aartsma, H. Michel, J. Köhler, Direct observation of tiers in the en-

ergy landscape of a chromoprotein: A single-molecule study, Proceedings of the National Academy of Sciences of the United States of America 100 (26) (2003) 15534–15538.

39. M. Brecht, H. Studier, A. F. Elli, F. Jelezko, R. Bittl, Assignment of red antenna states in photosystem I from Thermosynechoccocus elongatus by single-molecule spectroscopy, Biochemistry 46 (3) (2007) 799–806.

40. H. P. Lu, X. S. Xie, Single-molecule spectral fluctuations at room temperature, Nature 385 (6612) (1997) 143–146.

41. D. Rutkauskas, V. Novoderezhkin, R. J. Cogdell, R. van Grondelle, Fluorescence spectroscopy of conformational changes of single LH2 complexes, Biophysical Journal 88 (1) (2005) 422–435.

42. F. Schleifenbaum, C. Blum, V. Subramaniam, A. J. Meixner, Single-molecule spectral dynamics at room temperature, Molecular Physics 107 (18) (2009) 1923–1942.

43. Y. Berlin, A. Burin, J. Friedrich, J. Köhler, Low temperature spectroscopy of proteins. part ii: Experiments with single protein complexes, Physics of Life Reviews 4 (1) (2007) 64–89.

44. Y. Shibata, H. Ishikawa, S. Takahashi, I. Morishima, Time-resolved hole-burning study on myoglobin: Fluctuation of restricted water within distal pocket, Biophysical Journal 80 (2) (2001) 1013–1023.

45. C. Hofmann, M. Ketelaars, M. Matsushita, H. Michel, T. J. Aartsma, J. Köhler, Single-molecule study of the electronic couplings in a circular array of molecules: Light-harvesting-2 complex from rhodospirillum molischianum, Physical Review Letters 90 (1) (2003) 013004.

46. K. Huang, A. Rhys, Theory of light absorption and non-radiative transitions in f-centres, Proceedings of The Royal Society of London Series A-Mathematical and Physical Sciences 204 (1078) (1950) 406–423.

47. T. Pullerits, R. Monshouwer, F. van Mourik, R. van Grondelle, Temperature-dependence of electron-vibronic spectra of photosynthetic systems - computer-simulations and comparison with experiment, Chemical Physics 194 (2-3) (1995) 395–407.

48. I. Renge, Impurity spectroscopy in glasses and disordered crystals: Inhomogeneous broadening and electron phonon coupling, Journal of Luminescence 128 (3) (2008) 413–420.

49. M. Ratsep, M. Pajusalu, A. Freiberg, Wavelength-dependent electron-phonon coupling in impurity glasses, Chemical Physics Letters 479 (1-3) (2009) 140–143.

50. R. H. Austin, K. W. Beeson, L. Eisenstein, H. Fraunefelder, I. C. Gunsalus, Dynamics of ligand-binding to myoglobin, Biochemistry 14 (24) (1975) 5355–5373.

51. M. Brecht, H. Studier, V. Radics, J. B. Nieder, R. Bittl, Spectral diffusion induced by proton dynamics in pigment–protein complexes, Journal of the American Chemical Society 130 (51) (2008) 17487 – 17493.

52. M. Hussels, M. Brecht, Effect of glycerol and pva on the conformation of photosystem I, Biochemistry 50 (18) (2011) 3628–3637.

53. M. Hussels, M. Brecht, Evidence for direct binding of glycerol to photosystem I, Febs Letters 585 (15) (2011) 2445–2449.

54. P. Fromme, H. T. Witt, Improved isolation and crystallization of photosystem I for structural analysis, Biochim. Biophys. Acta, Bioenerg. 1365 (1-2) (1998) 175–184.

55. F. Müh, A. Zouni, Extinction coefficients and critical solubilisation concentrations of photosystems I and II from Thermosynechococcus elongatus, Biochim. Biophys. Acta, Bioenerg. 1708 (2) (2005) 219–228.

56. J. Pieper, J. Voigt, G. Renger, G. J. Small, Analysis of phonon structure in line-narrowed optical spectra, Chem. Phys. Lett. 310 (3-4) (1999) 296–302.

57. M. Ratsep, T. W. Johnson, P. R. Chitnis, G. J. Small, The red-absorbing chlorophyll *a* antenna states of photosystem I: A hole-burning study of Synechocystis sp PCC 6803 and its mutants, J. Phys. Chem. B 104 (4) (2000) 836–847.

58. A. C. M. Ferreon, M. M. Moosa, Y. Gambin, A. A. Deniz, Counteracting chemical chaperone effects on the single-molecule alpha-synuclein structural landscape, Proceedings of the National Academy of Sciences of the United States of America 109 (44) (2012) 17826–17831.

59. M. Ketelaars, J. M. Segura, S. Oellerich, W. P. F. de Ruijter, G. Magis, T. J. Aartsma, M. Matsushita, J. Schmidt, R. J. Cogdell, J. Kohler, Probing the electronic structure and conformational flexibility of individual light-harvesting 3 complexes by optical single-molecule spectroscopy, J. Phys. Chem. B 110 (37) (2006) 18710–18717.

60. D. Rutkauskas, J. Olsen, A. Gall, R. J. Cogdell, C. N. Hunter, R. van Grondelle, Comparative study of spectral flexibilities of bacterial light-harvesting complexes: Structural implications, Biophysical Journal 90 (7) (2006) 2463–2474.

61. L. Meinhold, J. C. Smith, A. Kitao, A. H. Zewail, Picosecond fluctuating protein energy landscape mapped by pressure-temperature molecular dynamics simulation, Proceedings of the National Academy of Sciences of the United States of America 104 (44) (2007) 17261–17265.

62. J. L. Silva, D. Foguel, C. A. Royer, Pressure provides new insights into protein folding, dynamics and structure, Trends In Biochemical Sciences 26 (10) (2001) 612–618.

63. P. H. Yancey, W. R. Blake, J. Conley, Unusual organic osmolytes in deep-sea animals: adaptations to hydrostatic pressure and other perturbants, Comparative Biochemistry and Physiology A-molecular and Integrative Physiology 133 (3) (2002) 667–676.

Table 1: Wavelength position and width of the average spectra for the different preparations given in Figure 3. Errors are due to CCD camera calibration. * Data taken from Ref. [52].

Matrix	wavelength position / nm	width / nm
H_2O	726.5±0.5	31.8±0.5
TMAO	727±1.0	32.2±0.5
Betaine	727.5±0.5	32.2±0.5
PVA 1%*	719±1.0	33.5±0.5
Glycerol 25%*	730±0.5	30.5±0.5
Glycerol 66%*	731±0.5	31.0±0.5

Table 2: Wavelength position and width of the ZPL distributions determined from data in Figure 7 by fitting with one Gaussian. * Data taken from Ref. [52].

Matrix	center position (nm)	σ (nm)	ZPL detection per PSI trimer (#)
H_2O	710.4	4.1	1.6
TMAO	710.2	4.1	0.7
Betaine	711.6	6.2	0.9
PVA 1%*	710.0	7.6	3.0
glycerol 25%*	709.9	3.1	1.2
glycerol 66%*	710.0	3.1	1.1

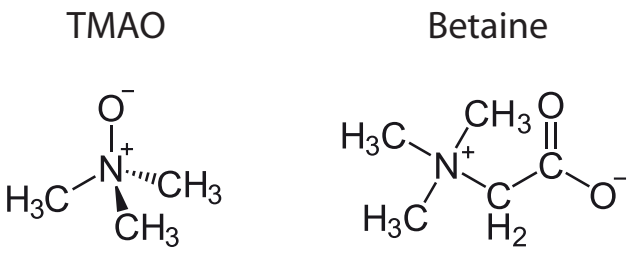

Figure 1: The two co-solvents investigated in this study: TMAO (pKa = 4.64.7; [6]) and betaine (pKa = 1.8; [25]). Both are zwitter ions in a wide pH range, including the values used in the described experiments.

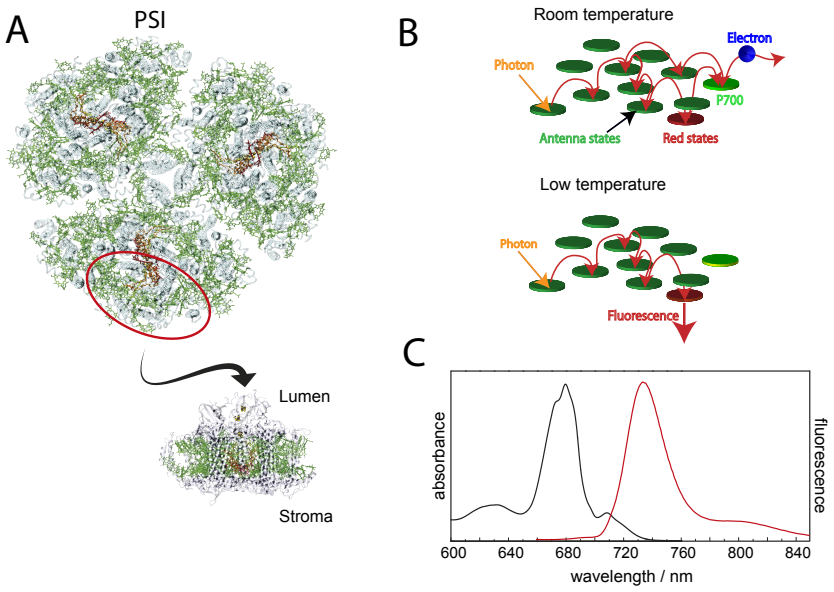

Figure 2: Photosystem I from oxygenic photosynthesis. A) Top view of trimeric PSI from cyanobacteria (protein data bank (PDB) entry: 1JB0)[31] together with a side view representation. In each monomer about 100 chlorophyll molecules (green) absorb excitation energy and transfer it to a chlorophyll dimer (red) in the reaction center absorbing at 700 nm (P700). The protein backbone is shown in violet. C) Illustration of excitation-energy transfer pathways at ambient and low temperatures. A charge-separated state across the membrane is formed upon excitation of P700. The red chlorophyll states are involved in energy transfer. At low temperatures the transfer toward P700 is partially blocked and the red chlorophyll states become fluorescent. E) Low-temperature (77 K) ensemble absorption and emission spectra of PSI of *T. elongatus* in the oxidized state adapted from Ref. [32].

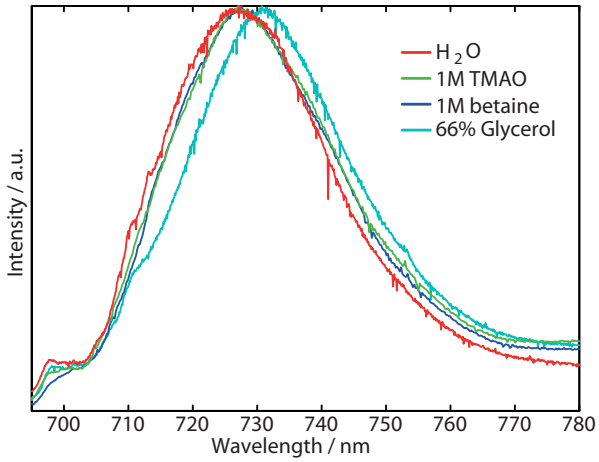

Figure 3: Averaged spectra obtained from the summation of 137 PSI trimers in buffer solution, 119 in TMAO solution, and 122 in betaine solution. For comparison, the average spectrum of 108 complexes taken in 66% glycerol/buffer taken from Ref. [52] is included. Data were scaled to similar amplitude.

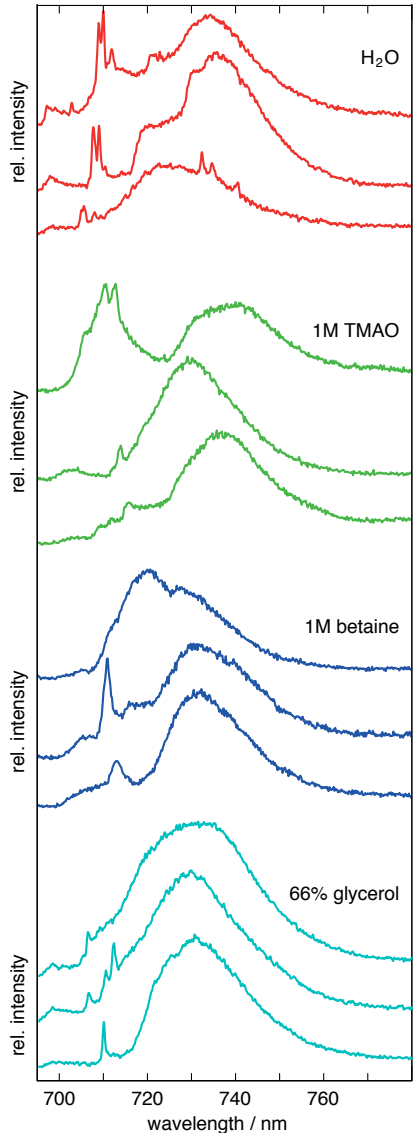

Figure 4: Fluorescence emission spectra of individual PSI complexes prepared in H_2O-based buffer solution (red), in 1M TMAO (green), and in 1M betaine (dark blue). For comparison of the effects of the co-solvents with the effect of glycerol on PSI emission, representative spectra of PSI in 66% glycerol taken from Ref.[53] have been included (cyan). Integration time per spectrum was between 100 s and 120 s , $\lambda_{exc} = 680\ nm; T = 1.4\ K$.

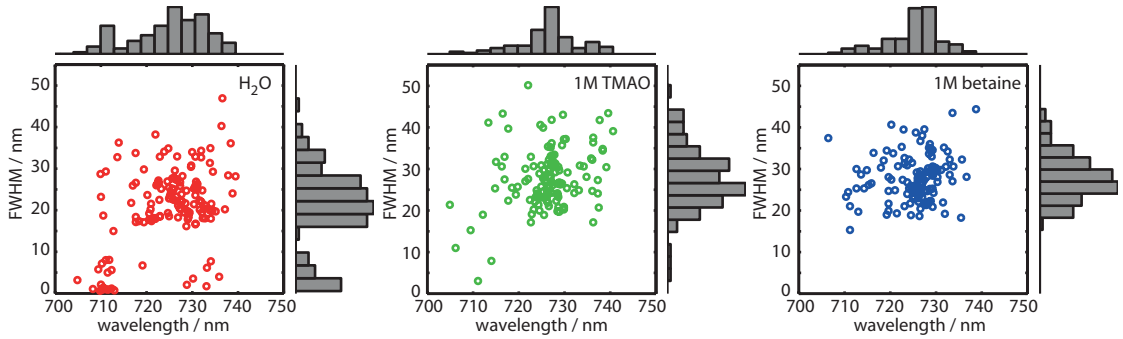

Figure 5: 2D-scatter-histogram plots obtained from the evaluation of the emission spectra of single PSI trimers in buffer solution, 1 M TMAO and 1 M betaine solution. Each dot represents the FWHM and wavelength position of the highest intensity peak in the spectra of the individual PSI complexes, as obtained by automated analysis (details see text).

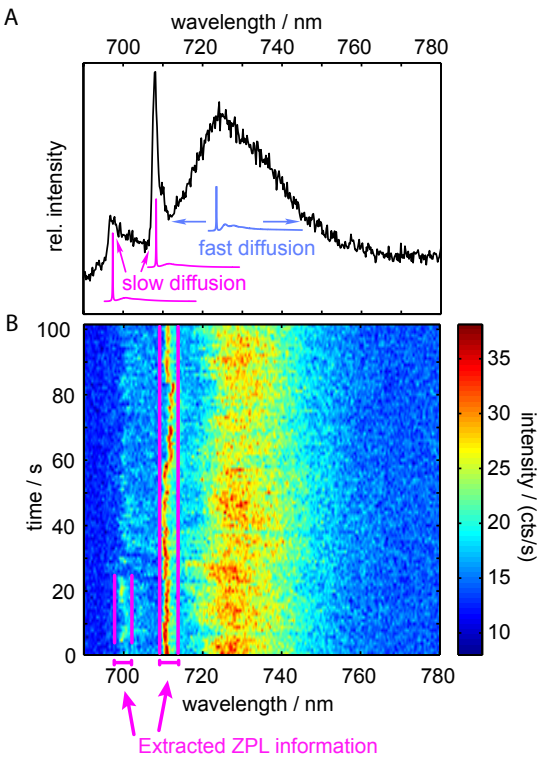

Figure 6: Time-dependent data and ZPL detection. a) The average spectrum over the time-dependent series of PSI spectra shows the characteristic contribution of the different red Chla emitters. Narrow ZPLs and broad contributions, which are associated to fast diffusing single emitters with a higher electron-phonon coupling. The theoretical line shapes of emitters without spectral diffusion are given in red. The line shapes were simulated by using the expressions and parameters in Refs. [56, 57]. b) Time-dependent spectral data of a single PSI in buffer and the result of automated ZPL identification. The typical data and results are shown. Time-dependent fluorescence emission spectra of individual PSI complexes from *T. elongatus* in TMAO. The accumulation time for the individual spectra was 1 s; $\lambda_{exc} = 680\ nm; T = 1.4\ K$.

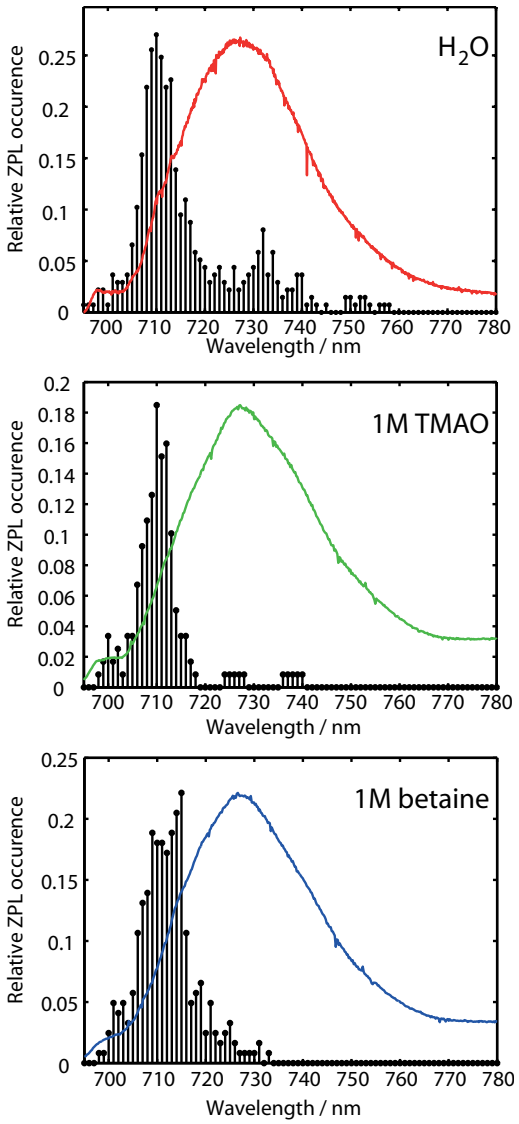

Figure 7: ZPL-histograms for PSI trimers in buffer solution, 1 M TMAO and 1 M betaine solution. The histograms are the result of an automated evaluation of time-dependent fluorescence emission spectra of single PSI trimers (for details see the Material and Methods in Ref. [52]). The average spectra of the different preparations are given in the background. The data were scaled to similar amplitude. Maximum position, width and total number of ZPLs are given in Table 2.

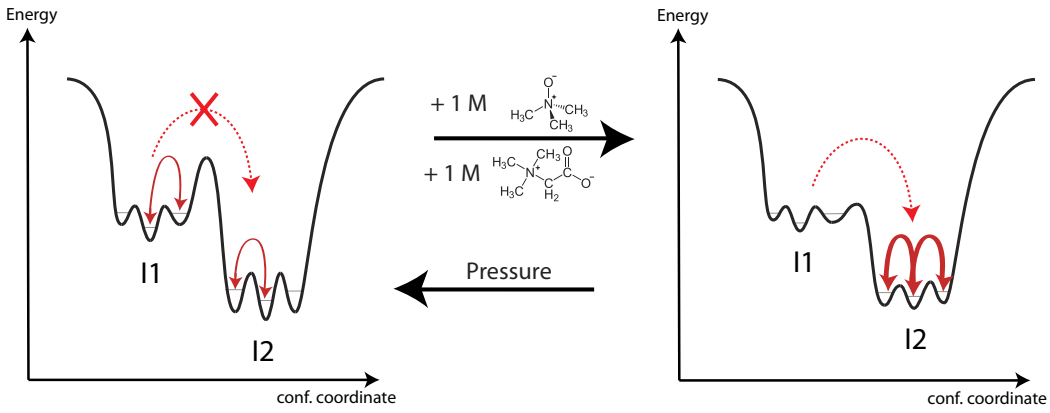

Figure 8: Schematic illustration of the protein energy landscape. (Left) Native condition. I1, I2 represent different intermediate states. (Right) The addition of TMAO or betaine to the buffer solution may reduce the height of the barriers separating the different local minima. Thereby the roughness of the energy landscape is reduced. Reducing the heights of the barriers enables a relaxation from S1 $\rightarrow$ S2 that is blocked under native conditions. This relaxation yields an increased homogeneity of the sample. The reduced barrier heights will increase spectral diffusion rates within I1 and I2. Application of pressure on proteins can change the curvature of the energy landscape in the opposite direction [61].